

Towards an Accurate and Secure Detector against Adversarial Perturbations

Chao Wang, Shuren Qi, Zhiqiu Huang,
Yushu Zhang, *Senior Member, IEEE*, and Xiaochun Cao, *Senior Member, IEEE*

Abstract—The vulnerability of deep neural networks to adversarial perturbations has been widely perceived in the computer vision community. From a security perspective, it poses a critical risk for modern vision systems, e.g., the popular Deep Learning as a Service (DLaaS) frameworks. For protecting off-the-shelf deep models while not modifying them, current algorithms typically detect adversarial patterns through discriminative decomposition of natural-artificial data. However, these decompositions are biased towards frequency or spatial discriminability, thus failing to capture subtle adversarial patterns comprehensively. More seriously, they are typically invertible, meaning successful defense-aware (secondary) adversarial attack (i.e., evading the detector as well as fooling the model) is practical under the assumption that the adversary is fully aware of the detector (i.e., the Kerckhoff's principle). Motivated by such facts, we propose an accurate and secure adversarial example detector, relying on a spatial-frequency discriminative decomposition with secret keys. It expands the above works on two aspects: 1) the introduced Krawtchouk basis provides better spatial-frequency discriminability and thereby is more suitable for capturing adversarial patterns than the common trigonometric or wavelet basis; 2) the extensive parameters for decomposition are generated by a pseudo-random function with secret keys, hence blocking the defense-aware adversarial attack. Theoretical and numerical analysis demonstrates the increased accuracy and security of our detector w.r.t. a number of state-of-the-art algorithms.

Index Terms—Adversarial example, detection, orthogonal decomposition, spatial-frequency, pseudo-random.

1 INTRODUCTION

MODERN deep neural networks are a powerful new technology, exhibiting impressive performance in extensive scenarios ranging from perceptual information understanding to hard scientific problem deciphering. Here, one typical class of network models is Convolutional Neural Networks (CNN), which are popular in semantic applications for visual data such as digital images. The effectiveness for such models is, in general, due to the highly discriminative and data-adaptive representation, technically enabled by the composition of numerous nonlinear transformations with learnable parameters [1].

Besides their effectiveness, the emerging Deep Learning as a Service (DLaaS) paradigm allows developers to apply or deploy proven network models in a simple and efficient manner [2]. The above two factors have led to the widespread emergence of deep learning-based artificial intelligence systems in everyday life, even expanding to many security and trust sensitive scenarios [3], e.g., self-driving cars, surveillance, drones and robotics, voice command recognition, and Face ID on mobile phones.

Despite the advantages w.r.t. discriminability, the robustness of deep neural networks has raised general concerns, especially in the computer vision community [4]. As a counter-intuitive vulnerability, it has been shown that *adversarial perturbations* on the input example can cause signifi-

cant fluctuations on such deep representations, even though such perturbations are quasi-imperceptible for humans [5].

Since the first work by Szegedy *et al.* [6], various attack methods have been proposed for well crafting such adversarial perturbations. In general, their design goals cover high fooling rate [7], low perceptual loss [8], efficient generation [9], high transferability w.r.t. models [10], high universality w.r.t. examples [11], less need for model knowledge [12], easy physical implementation [13], etc. Hence, these recent advances allow an adversary to perform effective evasion attacks at a low cost, which interfere in the deep representation and thus fundamentally destabilize the artificial system. In addition, the popularity of DLaaS-based development further increases this security threat. Specifically, a successful attack on few off-the-shelf deep models in DLaaS platform will affect a wide range of users and their systems, especially where safety-critical scenarios may be involved.

Integrating the above facts, it is generally agreed that adversarial perturbations have become a real threat that the security community has to face.

1.1 State of the Arts

For protecting deep neural networks and their application systems, some defense strategies towards adversarial attacks are designed over diverse research hypotheses and implementation paths.

The straightforward strategy is to include adversarial examples into the training, called *adversarial training*, which promotes the model learning and adapting to adversarial patterns [14]. It is somewhat effective in practice, but the re-training increases the implementation cost and the resulting

• C. Wang, S. Qi, Z. Huang, and Y. Zhang are with the College of Computer Science and Technology, Nanjing University of Aeronautics and Astronautics, Nanjing, China (e-mail: c.wang, shurenqi, zqhuang, yushu@nuaa.edu.cn).
• X. Cao is with the School of Cyber Science and Technology, Shenzhen Campus of Sun Yat-sen University, Shenzhen, China (e-mail: caoxiaochun@mail.sysu.edu.cn).

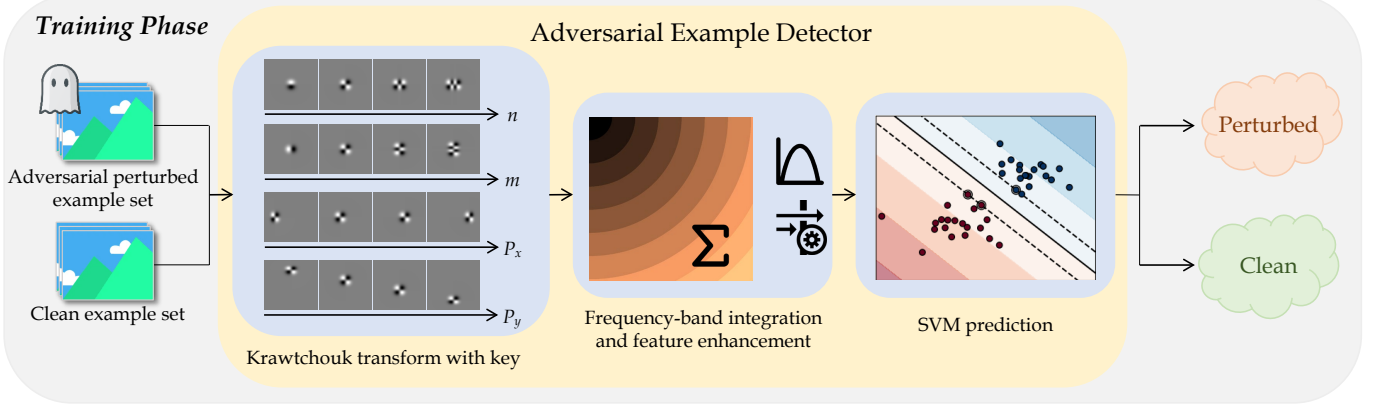


Fig. 1. Illustration for the training phase of the proposed adversarial example detector. The detector is trained on a set of adversarial/clean image examples along with corresponding labels. The detector consists of three main steps: 1) the image is projected into a space defined by Krawtchouk polynomials, where the frequency parameters (n, m) and spatial parameters (P_x, P_y) are determined by key; 2) the obtained coefficients are integrated and enhanced to form a compact-but-expressive feature vector by certain beneficial priors; 3) such features are fed into an SVM for the prediction, which is the only learning part in the detector.

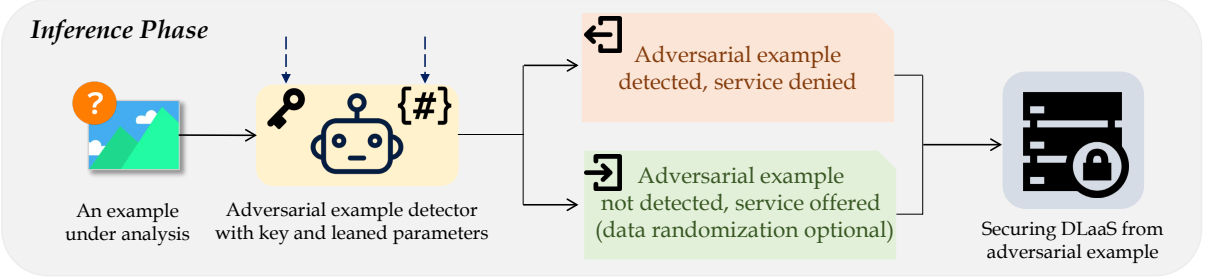


Fig. 2. Illustration for the inference phase of the proposed adversarial example detector. When the detector is trained (i.e., with the key and learned SVM parameters), it can be deployed in various real-world scenarios, where a DLaaS scenario is chosen as an example. For an image under analysis, our detector predicts whether it contains adversarial perturbations. With such prediction, the DLaaS is able to deny the service when the adversarial perturbation is revealed.

robustness cannot be adaptively/interpretable generalized to unseen adversarial patterns [15].

Another strategy seeks to add *regularization designs* in the network, e.g., regularization for layer [16], activation function [17], or loss function [18], thus embedding adversarial robustness priors into the network architecture. Ideally, such built-in designs have the potential to achieve adaptive/interpretable robustness against adversarial examples. Yet, in practice, tricky trade-offs between clean and robust accuracy are almost inevitable [19], and the additional cost for retraining is also significant.

As an alternative approach, *adversarial perturbation detector* is designed to reduce the clean-accuracy loss and additional implementation costs [20]. In general, it can serve as a pre-processing for off-the-shelf deep models to filter out potential adversarial examples, without modifying the model itself, being particularly suitable for DLaaS scenarios. Technically, such forensic detectors strongly relies on proper representation of the adversarial patterns while not being disturbed by the image contents, i.e., the discriminative decomposition of natural-artificial data [21], [22].

Here, the priori knowledge of adversarial perturbation is potentially useful to achieve such discriminative decomposition. In the learning of adversarial perturbation, the visual loss is usually limited by a regularization term; in

turn, forcing the perturbation to appear mainly in high frequency bands where the human visual system is less sensitive. Therefore, it is reasonable to assume that the adversarial examples have common frequency distribution pattern that differs from the natural examples, especially in high frequency bands.

From this assumption, researchers have tried to extract high-frequency discriminative features by various transformations, such as denoising filters [23], Spatial Rich Model (SRM) [24], Principal Component Analysis (PCA) [25], Discrete Cosine Transform (DCT) [26], Discrete Sine Transform (DST) [27], and Discrete Wavelet Transform (DWT) [27], with varying degrees of success.

1.2 Motivations

This line of adversarial perturbation detectors still falls short in accuracy and security, especially for real-world scenarios.

- For the *accuracy*, they are able to provide good detection performance when the scale of either the image patterns or the perturbation patterns is limited (e.g., MNIST with single kinds of attacks), while the accuracy degrades significantly when both are large [28]. This phenomenon implies that existing representation methods fail to capture subtle adversarial patterns comprehensively.

- As for the *security*, successful defense-aware (secondary) attack, i.e., evading the detector as well as fooling the model, is realistic under the Kerckhoffs's principle [29] — the adversary is fully aware of the detector. Technically, with the transparent definition of the decomposition, such perturbation can be learned by penalizing the specific features that the detector focuses on.

1.3 Contributions

Motivated by above facts, we attempt to present an accurate and secure adversarial example detector, technically enabled by a spatial-frequency discriminative decomposition with secret keys, as shown in Figs. 1 and 2. To the best of our knowledge, this is a very early work on fundamental improving both accuracy and security of detector from the basic decomposition stage.

- Regarding the *accuracy*, we first found that the failure for larger scale data may arise from the contradiction of spatial and frequency discriminability in the decomposition, surprisingly revisiting a classical problem of signal processing [30]. As an empirical case by Agarwal *et al.* [27], [28], a naive decision-level fusion of the DST (biased towards frequency) and DWT (biased towards spatial) is used to mitigate such contradiction partially. In this paper, we introduce Krawtchouk polynomials as basis functions for the discriminative decomposition, providing a mid-scale representation different from the global trigonometric basis in DST and the local wavelet basis in DWT. Note that such representation with rich spatial-frequency information can provide more clues of adversarial patterns for the prediction, being a more flexible detector than the decision-level fusion [27], [28].
- Regarding the *security*, we believe that the transparency of detector-interested features is the core for the successful defense-aware (secondary) attack, placing a foundational threat in many existing methods. In this paper, we propose a de-transparency strategy based on random feature selection [31]. More specifically, a pseudorandom number generator determines the spatial and frequency parameters of the decomposition, and the user controls such generator by setting the secret keys (i.e., the seed values). After such randomization, the defense-aware attack becomes difficult (or impossible) as the confusion of the boundary between to-be-attacked and to-be-evaded features, even for the adversary with the knowledge of the detector algorithm other than the keys.

2 RELATED WORKS

In this section, we review topics closely related to this paper, covering the generation, defense, and explanation of adversarial perturbations.

2.1 Generation of Adversarial Perturbations

The generation means finding a perturbation that has a small enough perceptual loss but can cause a large enough fluctuation in the output of the model [5]. In this regard, the researchers mainly focus on the objective definitions, perceptual metrics, and optimization algorithms.

2.1.1 Objective Definitions

Regarding the objective definition, it is a mathematical description for the goal of the generation. Therefore, the general definition is the combination of perceptual loss term (for visually reasonable) and model loss term (for high fooling rate) [5]. In the community, different scenarios and needs have led to a variety specific forms of this general definition. Here, in addition to the typical model loss for single model with single image [6], researchers are also seeking more efficient formalization of model loss for high transferability w.r.t. models [10], high universality w.r.t. examples [11], and less need for model knowledge [12].

As a more difficult term in the general definition, the perceptual loss term implies in fact the capturing of subjective visual perception through an objective metric. Next, we discuss it specially.

2.1.2 Perceptual Metrics

Regarding the perceptual metric, popular works are generally defined based on norms, with clear physical meanings. For example, the ℓ_∞ -norm constrains the largest magnitude among each element in the perturbation [9]; the ℓ_2 -norm constrains the Euclidean length of the perturbation [32]; the ℓ_1 -norm constrains the Manhattan length of the perturbation [32]; the ℓ_0 -norm constrains the number of perturbed pixels in the image [8]. From a visual perspective, the adversarial perturbations generated from norm-based perceptual metrics are generally non-semantic and appear similar to random noise.

More recently, several works explore a visually meaningful way for the generation of adversarial perturbations. Here, examples include visual watermarking [33], rain traces [34], out-of-focus blurring [35], and physically easy-to-implement patches [13]. Such attempts provide new insights into the generation of adversarial perturbations, further expanding the general definition of perceptual loss.

2.1.3 Optimization Algorithms

Regarding the optimization algorithm, it aims to discover the parameters in their space (generally very large) that enable the objective to hold. Therefore, the accuracy [6] and efficiency [9] of the solving are the core properties of interest to researchers. Here, popular optimization algorithms include single-step optimization [9], iterative optimization (especially gradient-based optimization) [7], and heuristic optimization [8], with varying accuracy and efficiency.

2.2 Defense against Adversarial Perturbations

The defense means protecting the model from adversarial attacks, or improving the performance of the model under adversarial attacks, with reasonable cost (in efficiency and accuracy) [20]. In this regard, the researchers mainly focus on the data-level defenses and the architecture-level defenses.

2.2.1 Data-level Defenses

Regarding the data-level defense, the most straightforward idea is *adversarial training* [14], where adversarial examples are included in the training. Empirically, this approach can significantly improve the robustness for the adversarial attacks seen in training. However, such robustness is not guaranteed for unseen attacks, and the model retraining often leads to a multiplicative increase in the training size [15].

Another idea is *data recovery* [36], where the perturbation patterns are reduced and the resulting recovered image is fed into a regular deep model. Here, by separating clean and perturbed data in the image, one can either directly remove the perturbed data (i.e., data compression) [37] or introduce randomness in the perturbed data to destroy their patterns (i.e., data randomization) [38]. Since discriminatively separating perturbed data and accurately reconstructing clean images are still open problems, this class of methods obviously faces a tricky accuracy-robustness tradeoff [19].

A similar idea to data recovery is the *adversarial perturbation detector* [20], it evaluates the likelihood of the presence of a perturbation in an image. Technically, such detector also relies on the discriminative decomposition of natural-artificial data, e.g., denoising filters [23], SRM [24], PCA [25], DCT [26], DST [27], and DWT [27]. Note that the accuracy-robustness tradeoff is largely avoided here, since such detector only excludes potential adversarial images without involving the lossy recovery for all input images. Hence, it is particularly suitable DLaaS scenarios [2], with promising overall performance on accuracy, robustness, and implementation cost.

2.2.2 Architecture-level Defenses

Regarding the architecture-level defense, deep models are redesigned to satisfy various mathematical constraints w.r.t. robustness priors, especially from the perspective of function continuity (e.g., Lipschitz continuity).

Typical efforts in this regard include the learnable denoising modules [39], the regularization for convolutional layers (e.g., with smooth kernels) [16], the regularization for activation functions (e.g., with stronger nonlinear properties) [17], and the regularization for loss functions (e.g., a new loss for penalizing model fluctuations) [18].

Ideally, such architecture-level efforts have the potential to achieve a built-in robustness against any adversarial examples with high confidence. In fact, however, these theory-driven designs face the same accuracy-robustness tradeoff. Owing to the lack of faithful and self-consistent explanation theory [40] for the behavior of deep models and the existence of adversarial examples.

2.3 Explanation for Adversarial Perturbations

The explanation means building a self-consistent theory to faithfully explain and predict adversarial phenomena [41]. In this regard, it is still controversial and no consensus theory has been developed in the community. A well-known case is the debate between Goodfellow *et al.* [9] and Tanay *et al.* [42] on the linear explanation.

Currently, researchers have proposed various explanations from training data (e.g., low sampling probability

assumption) [6], model structure (e.g., linear assumption) [9], manifold geometry (e.g., boundary tilting assumption) [42], and data features (e.g., high frequency and non-robust feature assumption) [43], [44].

In general, such theories generally agree only with their local observations, and it is possible to find counterexamples that invalidate them. Therefore, there still appears a long way to go for the faithful and self-consistent explanation theory.

3 GENERAL FORMULATION

In this section, we formulate the basic aspects involved in this paper, i.e., model, attack, and defense.

3.1 Model Formulation

We focus on deep convolutional neural network models for image classification tasks. Such classification models can be formulated as a mapping $\mathcal{M} : \mathcal{X} \rightarrow \mathcal{Y}$, where $\mathcal{X} \subset [0, 1]^{W \times H \times C}$ is the image space with image size $W \times H \times C$ and normalized pixel intensity $[0, 1]$; $\mathcal{Y} = \{1, 2, \dots, N\}$ is the label space with the category size N . For a clean data point $(\mathbf{x}, \mathbf{y}) \in \mathcal{X} \times \mathcal{Y}$, the classification model \mathcal{M} is considered to be correct if and only if $\mathcal{M}(\mathbf{x}) = \mathbf{y}$.

3.2 Attack Formulation

Attack objective. We focus on evasion attacks against above image classification models. For an image \mathbf{x} with the true label \mathbf{y} , the goal of the attacker is to find an adversarial perturbation δ such that:

$$\mathcal{M}(\mathbf{x} + \delta) \neq \mathbf{y}, \quad (1)$$

i.e., fooling the prediction, typically under a norm-based constraint for the imperceptibility of perturbation:

$$\|\delta\| < \varepsilon. \quad (2)$$

The resulting perturbed input for the model, i.e., the adversarial example, is denoted as $\mathbf{x}' = \mathbf{x} + \delta \in \mathcal{X}$. Note that the above attack objective is a formulation for the defense-unaware scenario, in line with the threat assumption of most related works. As for the defense-aware (secondary) attack, the goal of the attacker include the fooling of the adversarial perturbation detector: $\mathcal{D}(\mathbf{x}') = \mathcal{D}(\mathbf{x})$, in addition to the misclassification and imperceptibility above. Here, we denote the above defense-unaware and defense-aware attacks as $\mathcal{A}(\mathbf{x}) = \delta$. More detailed formulation on attacker and defender will be provided later.

Knowledge and capability. For the defense-unaware scenario, the attacker has perfect knowledge of the image classification model \mathcal{M} (i.e., full access to its mechanism and parameters), but has zero knowledge of the detector \mathcal{D} (or not aware of its presence). For the defense-aware scenario, the attacker likewise has perfect knowledge of the model \mathcal{M} and has limited knowledge of the detector \mathcal{D} — the attacker is aware the given model \mathcal{M} is being secured with a detector, knows its mechanism, but does not have access its secret keys. For both scenarios, the attacker has the capability to arbitrarily modify pixels within a given image \mathbf{x} .

3.3 Defense Formulation

Defense objective. The goal of our defense is to design an adversarial perturbation detector \mathcal{D} such that: $\mathcal{D}(\mathbf{x}) = 0$ (i.e., predicted as clean example) and $\mathcal{D}(\mathbf{x}') = 1$ (i.e., predicted as adversarial example) for any clean image $\mathbf{x} \in \mathcal{X}$ and corresponding adversarial example \mathbf{x}' by any pertinent \mathcal{A} . In other words, since \mathbf{x} and \mathbf{x}' differ only in δ , the above binary classification task is practically equivalent to a hypothesis testing for the presence of adversarial patterns (w.r.t. δ) under the strong interference from image content (w.r.t. \mathbf{x}).

4 TOWARDS ACCURATE AND SECURE DETECTOR: FORMULATION

In this section, we provide new formal analyses of the concerned accuracy and security issues, as the theoretical basis for the proposed detector.

4.1 Discriminability Analysis

The design of efficient detector \mathcal{D} relies heavily on a discriminative decomposition \mathcal{F} w.r.t. \mathbf{x} and δ in \mathbf{x}' . To achieve a high discriminability, two constraints are typically imposed on the explicit forms of \mathcal{F} .

Proposition 1. (Distributive Property of Addition). *The \mathcal{F} should be distributed over addition to fulfill: $\mathcal{F}(\mathbf{x}') = \mathcal{F}(\mathbf{x} + \delta) = \mathcal{F}(\mathbf{x}) + \mathcal{F}(\delta)$, i.e., the decomposition of the adversarial example is equivalent to the sum of the decomposition of the clean example and the perturbation.*

Such distributive property of addition facilitates the separation of natural-artificial data, and the terms like filtering [23], convolution [24], and inner product [26], [27] from successful detectors satisfy this property.

Proposition 2. (Statistical Regularity). *The $\mathcal{F}(\mathbf{x})$ is expected to exhibit a consistent statistical pattern for any clean image $\mathbf{x} \in \mathcal{X}$, and the $\mathcal{F}(\delta)$ is also expected to exhibit another consistent statistical pattern for any δ by pertinent \mathcal{A} ; meanwhile, such two statistical patterns should be significantly different.*

In order to better achieve the above statistical regularity, two priors of natural images and adversarial perturbations can be explored.

Proposition 3. (Frequency Prior). *For natural images, their local smoothness and nonlocal self-similarity nature leads to the dominance of low-frequency components [45]. For adversarial perturbations, the imperceptibility constraint drives the generated perturbations to contain mainly high-frequency components, due to the relative insensitivity of the human visual system to high-frequency information [43], [44].*

Proposition 4. (Spatial Prior). *For natural images, their high-frequency components are unevenly distributed over the image plane, depending on the semantic properties of image content. For adversarial perturbations, their high-frequency components are uniformly distributed over the image plane, since there is generally no term in the generation that controls the spatial distribution of the perturbations.*

Note that in the design of \mathcal{F} , both frequency and spatial properties are of interest. However, it is also well known that there is a trade-off between spatial and frequency resolutions of the orthogonal transform. In the related works, global transforms such as DST [27] bias towards frequency resolution, at the cost of spatial resolution. As the opposite, local transforms such as DWT [27] bias towards spatial resolution, at the cost of frequency resolution. Therefore, neither of them can provide rich spatial-frequency information.

Motivated by above facts, we introduce a mid-scale representation based on Krawtchouk polynomials, which provides a well trade-off between spatial and frequency resolutions than global/local transforms.

4.2 Security Analysis

Assuming that \mathcal{F} decomposes the input image into a set of coefficients \mathcal{C} : $\mathcal{F}(\cdot) = \mathcal{C}$. Suppose the adversarial perturbations generated by (1) and (2) have a strong response (with main energy) on a subset of coefficients: $\mathcal{C}_A \subset \mathcal{C}$, and the detector-interested (with higher weights) subset of coefficients is denoted as $\mathcal{C}_D \subset \mathcal{C}$. Therefore, the effectiveness of detector \mathcal{D} is in fact built on the intersection $\mathcal{C}_A \cap \mathcal{C}_D$, where we denote the corresponding coefficient subset for a perturbation δ as $\mathcal{F}_{\mathcal{C}_A \cap \mathcal{C}_D}(\delta)$.

Proposition 5. (Defense-aware Attack: General Objective). *With the above assumptions and notations, the objective of the defense-aware attack can be modeled on the correlation ρ :*

$$\rho(\mathcal{F}_{\mathcal{C}_A \cap \mathcal{C}_D}(\delta_{\text{old}}), \mathcal{F}_{\mathcal{C}_A \cap \mathcal{C}_D}(\delta_{\text{new}})) < \eta, \quad (3)$$

for an image \mathbf{x} , with also objectives (1) and (2), where δ_{old} is the generated perturbation in the defense-unaware scenario, i.e., by only (1) and (2), and δ_{new} is the perturbation being generated.

Proposition 6. (Defense-aware Attack: A Special Case). *In practice, objective (3) can be converted into another easily implemented objective — directly shifting the main energy of the perturbation δ_{new} out of $\mathcal{C}_A \cap \mathcal{C}_D$:*

$$\|\mathcal{F}_{\mathcal{C}_A \cap \mathcal{C}_D}(\delta_{\text{new}})\| < \lambda, \quad (4)$$

such an objective allows defense-aware perturbations to form on the relative complement $\mathcal{C} \setminus (\mathcal{C}_A \cap \mathcal{C}_D)$, hence destroying the consistent pattern of $\mathcal{F}(\delta_{\text{old}})$ and $\mathcal{F}(\delta_{\text{new}})$ on the adversarial and detector-interested $\mathcal{C}_A \cap \mathcal{C}_D$.

Note that above new objectives in the defense-aware scenario, i.e., (3) or (4), rely in fact on the sufficient knowledge of detector \mathcal{D} and decomposition \mathcal{F} . Under the Kerckhoffs's principle, we assume that the adversary has such knowledge (see also Section 3.2), which is practical due to the transparency in the design of \mathcal{D} and the definition of \mathcal{F} for many related works [23] ~ [27]. With such knowledge, the adversary is able to identify the critical $\mathcal{C}_A \cap \mathcal{C}_D$ and hence successfully evade the detector \mathcal{D} as well as fool the model \mathcal{M} by the objectives (1) and (2) with (3) or (4).

Motivated by above facts, we introduce a de-transparency strategy on \mathcal{F} by random feature selection with keys, which confusion of the boundary between to-be-attacked features $\mathcal{C} \setminus (\mathcal{C}_A \cap \mathcal{C}_D)$ and to-be-evaded features $\mathcal{C}_A \cap \mathcal{C}_D$.

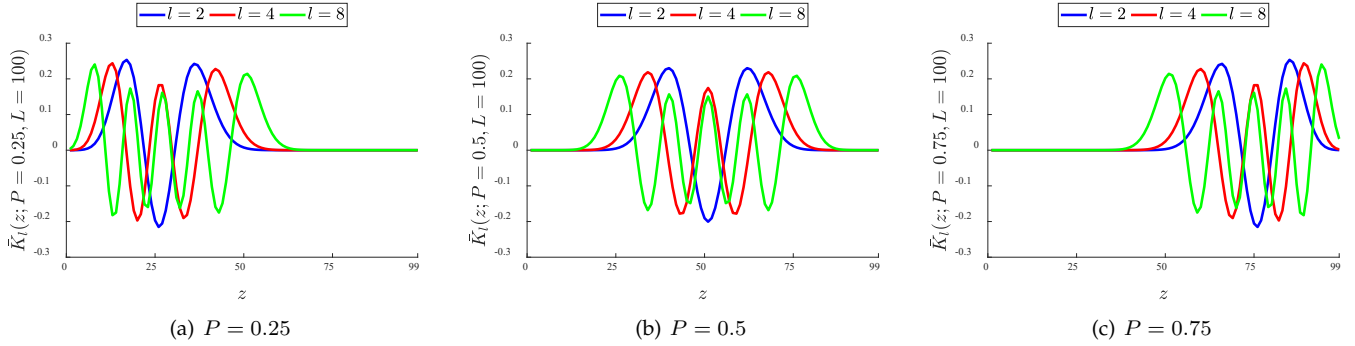


Fig. 3. Illustration for the weighted Krawtchouk polynomials $\tilde{K}_l(z; P, L)$ with $l = \{2, 4, 8\}$, $P = \{0.25, 0.5, 0.75\}$, and $L = 100$. Note that the number and location of zeros of \tilde{K} can be adjusted explicitly by l and P , respectively, meaning the time-frequency discriminability of the represented image information.

5 TOWARDS ACCURATE AND SECURE DETECTOR: METHODOLOGY

In this section, we specify the proposed detector against adversarial perturbation. We will first give an overview drawing a high-level intuition for readers, and then the main techniques within the methodology are presented separately.

5.1 Overview

In general, the proposed detector consists of three main steps, going through training and inference phases.

As shown in Fig. 1, the training of our detector aims to fit a mapping from a set of adversarial/clean image examples to the corresponding labels. For an efficient mapping, our detector is equipped with three steps that perform decomposition, featuring, and classification, respectively.

- Regarding the *decomposition*, the image is projected into a space defined by Krawtchouk polynomials, in which the clean image \mathbf{x} and adversarial perturbation δ are better separable from \mathbf{x}' (see also the discriminability analysis in Section 4.1). As for security, the frequency parameters (n, m) and spatial parameters (P_x, P_y) are determined by the user key, which is considered as a de-transparent mechanism for decomposition (see also the security analysis in Section 4.2). The description on decomposition will be presented in Section 5.2.
- Regarding the *featuring*, a compact-but-expressive feature vector is formed on the obtained decomposition coefficients. Here, the statistical regularity in the frequency and spatial domains are introduced, where coefficients are integrated and enhanced as feature by means of above beneficial priors. The description on featuring will be presented in Section 5.3.
- Regarding the *classification*, the above features are fed into a Support Vector Machine (SVM) for an automatic two-class separation of feature space. Note that the decomposition and featuring are non-learning, and the SVM is the only learning part of the detector. The description on classification will be presented in Section 5.4.

As shown in Fig. 2, the trained detector is an accurate and secure defense tool against adversarial attacks, technically enabled by a spatial-frequency discriminative decomposition with secret keys. It can be deployed in various real-world scenarios, where a DLaaS scenario is chosen as an example. For an image under analysis, our detector (with the same key and SVM parameters in training) predicts whether it contains adversarial perturbations. By such prediction, the DLaaS is able to deny the service when the adversarial perturbation is revealed.

5.2 Spatial-frequency Discriminative Decomposition with Secret Keys

Our defense framework starts with a spatial-frequency discriminative decomposition of input example. In this subsection, we discuss the explicit definition of such decomposition, as well as the security enhancement strategy with secret keys.

Definition 1. (Orthogonal Decomposition). The orthogonal decomposition of an image function $f \in \mathcal{X}$, denoted as \mathcal{F} , is defined as the inner product of the image function f and the basis function V [46]:

$$\mathcal{F}(f) = \iint_D V_{nm}^*(x, y) f(x, y) dx dy, \quad (5)$$

where the frequency parameters $(n, m) \in \mathbb{Z}^2$, the domain of basis function $D \subset \{(x, y) \in \mathbb{R}^2\}$, the asterisk $*$ denotes the complex conjugate. Here, the basis function V satisfy orthogonality over the domain D as:

$$\iint_D V_{nm}(x, y) V_{n'm'}^*(x, y) dx dy = \delta_{nn'} \delta_{mm'}, \quad (6)$$

where δ is the Kronecker delta function: $\delta_{ab} = [a = b]$.

With the Definition 1, one can note that the orthogonal decomposition methods used in existing detectors all have the form (5) and (6), and their difference lies in the definition of the basis function V . For example, the DST and DWT in the detector of Agarwal *et al.* [27] are with the global trigonometric basis and local wavelet basis, respectively. In this paper, we define a mid-scale basis by Krawtchouk polynomials for a better trade-off between spatial and frequency resolutions.

Definition 2. (Krawtchouk Basis). The Krawtchouk basis function V is defined as [47]:

$$V_{nm}(x, y) = \bar{K}_n(x; P_x, W) \bar{K}_m(y; P_y, H), \quad (7)$$

where domain of basis function $D = \{(x, y) \in [0, 1, \dots, W] \times [0, 1, \dots, H]\}$ with image size $W \times H$, frequency parameters $(n, m) \in [0, 1, \dots, W] \times [0, 1, \dots, H]$, spatial parameters $(P_x, P_y) \in (0, 1)^2$, and weighted Krawtchouk polynomials \bar{K} are defined as:

$$\bar{K}_l(z; P, L) = \sqrt{\frac{\binom{L}{z} P^z (1-P)^{L-z}}{(-1)^l \left(\frac{1-P}{P}\right)^l l! \Gamma(-L) \Gamma(l-L)}} {}_2F_1(-l, -z; -L; \frac{1}{P}), \quad (8)$$

where hypergeometric function ${}_2F_1$ is defined as:

$${}_2F_1(a, b; c; d) = \sum_{k=0}^{\infty} \frac{(a)_k (b)_k}{(c)_k} \frac{d^k}{k!}, \quad (9)$$

with Pochhammer symbol: $(a)_k = \Gamma(a+k)/\Gamma(a)$. For more efficient computation of (8), i.e., avoiding the infinite summation in (9), we introduce the recursive formula for weighted Krawtchouk polynomials \bar{K} :

$$\begin{aligned} \bar{K}_{l+1} &= \frac{\sqrt{\frac{(1-P)(l+1)}{P(L-l)}} (LP - 2lP + l - z) \bar{K}_l}{P(l-L)} \\ &\quad - \frac{\sqrt{\frac{(1-P)^2(l+1)l}{P^2(L-l)(L-l+1)}} l(1-P) \bar{K}_{l-1}}{P(l-L)}, \end{aligned} \quad (10)$$

with initial items \bar{K}_1 and \bar{K}_0 :

$$\bar{K}_1(z; P, L) = (1 - \frac{z}{PL}) \bar{K}_0, \quad (11)$$

$$\bar{K}_0(z; P, L) = \sqrt{\binom{L}{z} P^z (1-P)^{L-z}}. \quad (12)$$

By substituting the basis of Definition 2 into the decomposition of Definition 1, we have formulated the Krawtchouk decomposition, which is fundamental in our detector.

5.2.1 Discriminability Analysis

Next, we will discuss the key property of Krawtchouk decomposition, i.e., time-frequency discriminability, and its role in the detection of adversarial perturbation.

Property 1. (Time-frequency Discriminability). The frequency and spatial properties of the represented image information by Krawtchouk decomposition can be controlled with the frequency parameters (n, m) and spatial parameters (P_x, P_y) , respectively.

Remark. In the study of image representation, it has been found that the frequency and spatial properties of orthogonal decomposition rely on the number and location of zeros of the basis functions, respectively [48]. Specific to this paper, the core of time-frequency discriminability in Krawtchouk decomposition is that the number and location of zeros can be adjusted explicitly by (n, m) and (P_x, P_y) , respectively.

- The number of zeros of the 1D $\bar{K}_l(z; P, L)$ is proportional to l . As for the 2D $V_{nm}(x, y) = \bar{K}_n(x) \bar{K}_m(y)$, similar conclusion holds w.r.t. the n and m at the x -direction and y -direction, respectively.
- The location of zeros of the 1D $\bar{K}_l(z; P, L)$ is biased towards 0 when $P < 0.5$, uniform when $P = 0.5$, and biased towards 1 when $P > 0.5$, where the more deviation of P from 0.5 is, the more biased the distribution of zeros is. As for the 2D $V_{nm}(x, y) = \bar{K}_n(x) \bar{K}_m(y)$, similar conclusion holds w.r.t. the P_x and P_y at the x -direction and y -direction, respectively.

In Fig. 3, we illustrate 1D plots of weighted Krawtchouk polynomials $\bar{K}_l(z; P, L)$ for a high-level intuition of such time-frequency discriminability. Here, the plots under different parameter settings: $l = \{2, 4, 8\}$ and $P = \{0.25, 0.5, 0.75\}$ with $L = 100$. As can be expected, changing l will change the number of zeros of \bar{K} , which in turn corresponds to a change in the frequency properties. As for P , the change of its value will change the distribution of zeros, which in turn corresponds to a change in the spatial properties. The 2D plots of $V_{nm}(x, y)$ w.r.t. (n, m) and (P_x, P_y) are given in Fig. 1, where frequency and spatial property changes at the x and y directions can be observed.

Main Result 1. (Discriminability for Adversarial Perturbation). The Krawtchouk decomposition is claimed to be discriminative for adversarial perturbation due to the following factors: 1) The Krawtchouk decomposition defined by the inner product (Definitions 1 and 2) satisfies the distributive property of addition (Proposition 1); 2) The Krawtchouk decomposition with time-frequency discriminability (Property 1) exhibits potential in exploring the statistical regularity (Proposition 2), when the frequency prior (Proposition 3) and spatial prior (Proposition 4) hold in natural images and adversarial perturbations.

Remark. Although decompositions in competing detectors, e.g., denoising filters [23], SRM [24], DCT [26], DST [27], and DWT [27], all satisfy the distributive property of addition (Proposition 1), achieving the statistical regularity (Proposition 2) is still an open problem. Global decompositions, e.g., DST, are biased towards frequency resolution, thus better exploiting frequency priors, but fail in mining spatial priors. In contrast, local decompositions, e.g., denoising filters, SRM, and DWT, can fully exploit the spatial prior, but only provide limited frequency resolution and thus fail in mining frequency priors. As a mid-scale representation, the Krawtchouk decomposition provides a well trade-off between spatial and frequency resolutions than above global/local methods. It is thus expected to reveal a more comprehensive pattern of adversarial perturbation over the both spatial and frequency dimensions.

5.2.2 Security Analysis

With the Property 1 and the Main Result 1, we have analyzed the theoretical effectiveness of the Krawtchouk decomposition in detecting adversarial perturbations. Next, we will discuss the de-transparency strategy of decomposition to provide certain security guarantees against defense-aware (secondary) attacks.

In the implementation of previous detector, the parameters of the orthogonal decomposition were often determined *explicitly* by the user. In our implementation, the frequency parameters (n, m) and spatial parameters (P_x, P_y) are determined by a pseudorandom number generator, i.e., random feature selection [31]. Note that the random numbers will be appropriately scaled and quantized to fit the physical meaning of these parameters, i.e., within the domains $[0, 1, \dots, W] \times [0, 1, \dots, H]$ and $(0, 1)^2$, respectively. The user keeps the seed value of the generator secret, where such seed is considered as the key for decomposition. In fact, the secret key determines the set of coefficients (w.r.t. spatial and frequency features) that the detector can explore, and hence changing the key will result in a different detector (see also Property 1).

Main Result 2. (Security for Defense-aware Attack). *The random feature selection is claimed to be security for defense-aware attack due to the following factor. After the randomization of Krawtchouk decomposition, the adversary is difficult (or impossible) to identify the adversarial and detector-interested $\mathcal{C}_A \cap \mathcal{C}_D$ (Propositions 5 and 6), even with the knowledge of the detector algorithm other than the keys. Furthermore, such de-transparency strategy confusion of the boundary between to-be-attacked features $\mathcal{C} \setminus (\mathcal{C}_A \cap \mathcal{C}_D)$ and to-be-evaded features $\mathcal{C}_A \cap \mathcal{C}_D$, resulting in a dilemma for the adversary in attacking the model \mathcal{M} and evading the detector \mathcal{D} .*

Remark. Some decompositions in competing detectors, e.g., denoising filters [23] and SRM [24], are based on a few fixed filters/bases. Such design is easy for the adversary to form an effective evasion of the detector. Other detectors use a more comprehensive bases as the decomposition, e.g., DCT [26], DST [27], and DWT [27], which intuitively enhances both the discriminability and security. However, the risk of evading the detector remains, where the adversary can still determine the critical $\mathcal{C}_A \cap \mathcal{C}_D$ due to the transparency in the design of detector and the definition of decomposition. In our work, the random feature selection provides a well de-transparency mechanism, placing fundamental dilemma for the defense-aware attack.

5.3 Frequency-band Integration and Feature Enhancement

We first recall Section 5.2 and provide some proper notations. After the Krawtchouk decomposition, the set of spatial-frequency discriminability (Result 1) coefficients is denoted as $\mathcal{C} = \{c_{n,m,P_x,P_y}\}$, where the random feature selection provides certain security guarantees w.r.t. defense-aware attacks (Result 2). In the implementation, we prefer to sample a few spatial parameters (P_x, P_y) but sample a large number of frequency parameters (n, m) . It allows for capturing the potential adversarial patterns as comprehensively as possible while bounding the complexity.

Frequency-band Integration. With the sampling strategy of the parameters, the coefficient set \mathcal{C} is very high-dimensional and exhibits certain information redundancy, where direct knowledge engineering is usually inefficient. Here, the statistical regularity (Proposition 2) are explored for forming a compact-but-expressive feature vector \mathcal{V} on

the coefficient set \mathcal{C} . More specifically, the coefficients of similar frequency properties in \mathcal{C} are integrated as a component of feature vector \mathcal{V} , inspired by the frequency prior (Proposition 3) and spatial prior (Proposition 4). First, the space of frequency coefficients of the Krawtchouk decomposition, i.e., $(n, m) \in [0, 1, \dots, W] \times [0, 1, \dots, H]$, is divided equally into $\#_B$ bands under ℓ_2 norm:

$$\mathcal{B}_i = \{(n, m) : \frac{i-1}{\#_B} \|(W, H)\|_2 \leq \|(n, m)\|_2 < \frac{i}{\#_B} \|(W, H)\|_2\}, \quad (13)$$

where $i = 1, 2, \dots, \#_B$ and $\mathcal{C} = \bigcup_{i=1}^{\#_B} \mathcal{B}_i$.

Then, the coefficients c_{n,m,P_x,P_y} in the frequency band \mathcal{B}_i are considered with similar frequency properties and they are integrated as a feature component:

$$\mathcal{V}_i(P_x, P_y) = \sum_{(n,m) \in \mathcal{B}_i} c_{n,m,P_x,P_y}, \quad (14)$$

where the feature vector $\mathcal{V} = \{\mathcal{V}_i(P_x, P_y)\}$.

Feature Enhancement. In fact, the feature \mathcal{V} obtained by frequency-band integration can still be enhanced, i.e., improving compactness and expressiveness. Here, we present two simple enhancement strategies, note that they are optional and not mandatory in the implementation.

- **Weighting:** Starting from pairs of clean and adversarial examples in the training set, we evaluate in which frequency bands the features exhibit stronger variability. Simple functions (e.g. Gaussian functions) reflecting such variability can be set to weight the obtained feature vector, where the more discriminative bands are highlighted.
- **Ranking:** Starting from the features and labels of the training examples, we calculate the correlation of each feature dimension/component with the labels. Then, the feature vector is re-ranked according to the relevance, where the dimension/component with low relevance can be dropped directly.

5.4 SVM Prediction

After the featuring of Section 5.3, we formed compact-but-expressive feature \mathcal{V} from the Krawtchouk coefficient set \mathcal{C} . Considering the discriminative power of such features, a simple SVM classification model is sufficient to support a two-class separation of feature space. Since the SVM prediction is not our main technical contribution, only a brief description is provided.

Here, a set of paired clean-adversarial image examples is employed as the training set. The features formed on training set and corresponding labels are fed into a SVM. The training process attempt to achieve a proper mapping from features to labels by minimizing the loss. The learned SVM parameters are then saved as an important part of the detector, and such parameters will be shared to the inference phase of the practical deployment. Note that the SVM is the only learning part of the detector.

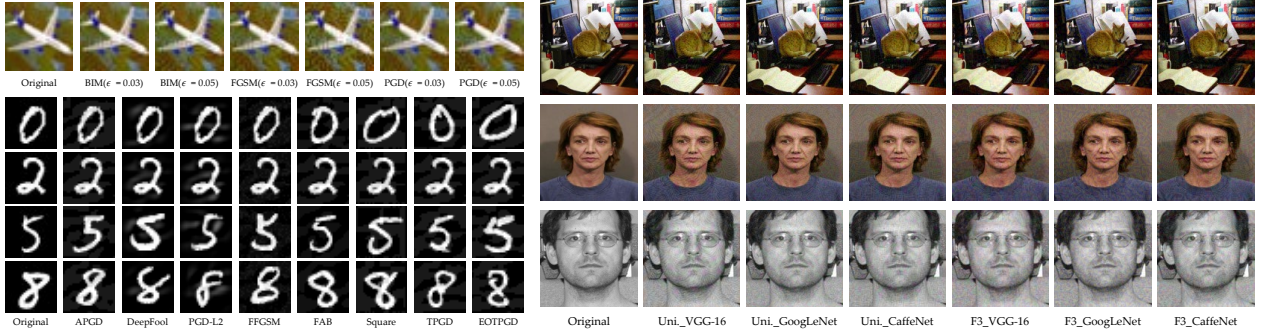


Fig. 4. Illustration for the datasets and adversarial attacks involved in experiments.

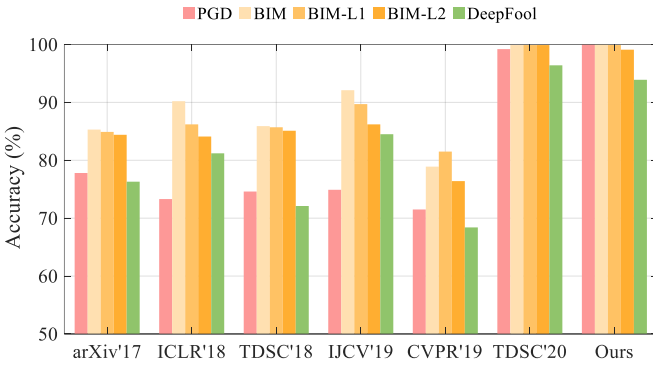


Fig. 5. The benchmarking of adversarial perturbation detection accuracy for different detectors on the MNIST dataset.

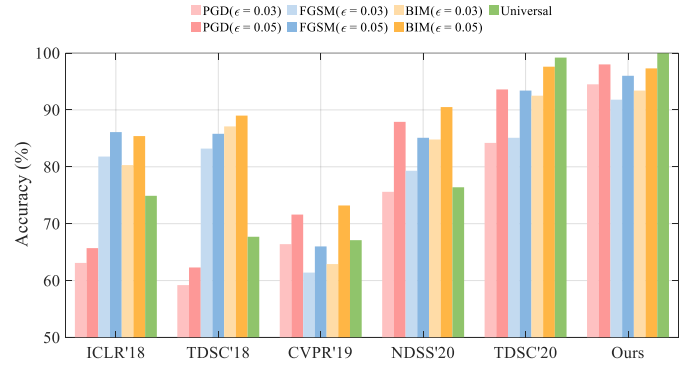


Fig. 6. The benchmarking of adversarial perturbation detection accuracy for different detectors on the CIFAR-10 dataset.

6 EXPERIMENTS

In this section, we will evaluate the capability of the proposed method to detect adversarial examples by extensive quantitative analysis. We first provide the basic setup w.r.t. models, attacks, and defenses in the following experiments. Then, the proposed detector is evaluated with benchmarking, crossing, and challenging protocols, thus determining its position w.r.t. current state-of-the-art detectors and its effectiveness for realistic scenarios.

6.1 Experiment Setup

In general, the experiments of this paper involve the setup of three aspects: 1) the foundational deep models along with datasets, which are going to be attacked/defended; 2) the adversarial perturbation generators for attacking; 3) the adversarial perturbation detectors for defending. In Fig. 4, we provide the visualization for some adversarial images.

The deep models involved in experiments are

- LeNet [49];
- VGG-16 [50];
- GoogLeNet [51];
- CaffeNet [52].

The datasets involved in experiments are

- MNIST [53], a large dataset of handwritten digits;
- CIFAR-10 [54], a large dataset of small-size color images;
- MEDS [55], a face image dataset;

- Multi-PIE [56], a face image dataset;
- PubFig [57], face image dataset;
- ImageNet [58], a very large dataset of natural image.

The adversarial attacks involved in experiments are

- FGSM [9], i.e., Fast Gradient Sign Method with variants of L1 and L2 norms;
- BIM [7], i.e., Basic Iterative Method, as an iterative version of FGSM also with variants of L1 and L2 norms;
- PGD [59], i.e., Projected Gradient Descent, with variants of L2 norm;
- APGD [60], i.e., Auto PGD;
- DeepFool [61];
- FFGSM [62], i.e., Fast adversarial training using FGSM;
- FAB [63], i.e., Fast Adaptive Boundary;
- Square [64], i.e., a black-box attack based on square-shaped updates;
- TPGD [65], i.e., Theoretically principled PGD;
- EOTPGD [66], i.e., Expectation Over Transformation and PGD;
- Universal [11], i.e., a perturbation can attack images universally;
- F3 [67], i.e., Fast Feature Fool, as also a universal perturbation.

The adversarial perturbation detectors (i.e., comparison methods) involved in experiments are

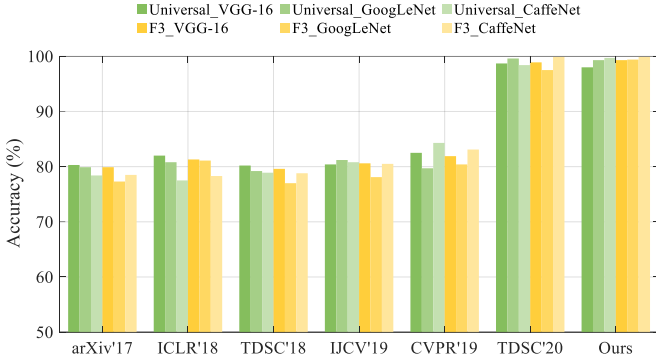


Fig. 7. The benchmarking of adversarial perturbation detection accuracy for different detectors on the MEDS dataset.

- arXiv'17 [68] by looking at Bayesian uncertainty estimates;
- ICLR'18 [69] by detecting out-of-distribution images;
- TDSC'18 [23] by denoising filters;
- IJCV'19 [70] by characterizing abnormal filter response behavior;
- CVPR'19 [24] by steganalysis and spatial rich model;
- NDSS'19 [71] by neural network invariant checking;
- TDSC'20 [27] by global and local orthogonal decomposition.

Note that the results for above comparison methods in following experiments are mainly cited from [27].

6.2 Benchmarking Experiments

In this part, we provide benchmarking evaluations of the proposed detector w.r.t. current state-of-the-art detectors, under the typical experimental protocol in these related works.

6.2.1 MNIST

Fig. 5 shows the accuracy comparison of 7 detectors w.r.t. 7 attacks on the MNIST dataset. Here, 9000 clean images are selected from the MNIST, and then 9000 corresponding perturbed images are formed by each attack. For each competing detector, it is trained and tested based on the above images, with a training-testing split of 50%-50% on both original and perturbed images. It can be observed that both TDSC'20 and proposed detectors achieve significant gains in detection accuracy w.r.t. other advanced detectors over different attacks. A possible explanation is that the orthogonal decomposition provides more comprehensive representations of perturbations for the classifier.

6.2.2 CIFAR-10

Fig. 6 shows the accuracy comparison of 6 detectors w.r.t. 7 attacks on the CIFAR-10 dataset. Here, the experiment covers 10000 clean images and 10000 corresponding perturbed images for each attack, also with 50%-50% training-testing split. Compared to the results on MNIST, one can note a significant performance degradation in competing methods, even >10% degradation in ICLR'18 and TDSC'18 w.r.t. PGD attacks. This is mainly due to the richer patterns of image content in CIFAR-10, which acts as a strong interference for

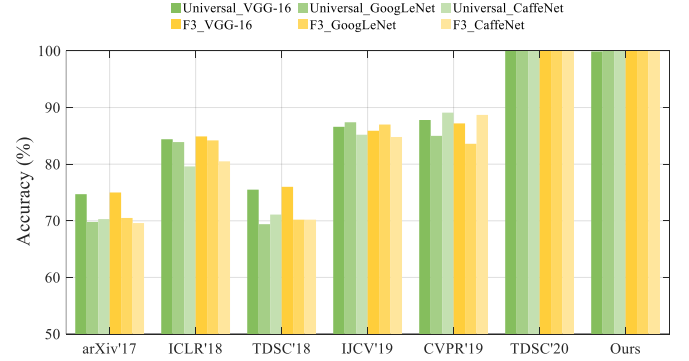


Fig. 8. The benchmarking of adversarial perturbation detection accuracy for different detectors on the Multi-PIE dataset.

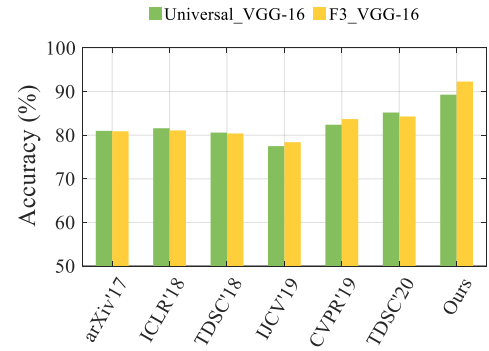


Fig. 9. The benchmarking of adversarial perturbation detection accuracy for different detectors on the ImageNet dataset.

representing perturbation patterns. Among them, the proposed detector exhibits the least performance degradation over different attacks, even when compared to TDSC'20. Such a phenomenon further confirms the effectiveness of our spatial-frequency discriminative decomposition.

6.2.3 MEDS and Multi-PIE

In Fig. 7 and Fig. 8, we provide accuracy comparison of 7 detectors w.r.t. 6 attacks on face datasets MEDS and Multi-PIE, respectively. Here, universal perturbation is imposed on small-scale face images, with 50%-50% training-testing split, where both perturbation and content patterns are relatively homogeneous. Even under this protocol, none of the competing methods except TDSC'20 achieved > 90% detection accuracy. This implies that non-complete image representations are not sufficient for supporting an efficient detector, even in small-scale detection scenarios. Under such simple experimental protocol, both the proposed detector and TDSC'20 exhibit ~ 100% accuracy, in line with general expectations of this paper.

6.2.4 ImageNet

As for Fig. 9, the accuracy comparison of 7 detectors w.r.t. 2 attacks on ImageNet dataset is illustrated. Here, universal perturbation is imposed on large-scale natural images, also of 50%-50% training-testing split. Clearly, the diversity of the image content increases significantly w.r.t. the previous experimental protocol, increasing also the difficulty of the detection. An interesting phenomenon is that the gap

TABLE 1

Recall, Precision, F1, and Accuracy Scores (%) of Crossing Dataset Experiments.

Training	Testing	Recall	Precision	F1	Accuracy
MEDS	Multi-PIE	100.00	100.00	100.00	100.00
	PubFig	99.91	99.86	99.88	99.88
Multi-PIE	MEDS	100.00	91.52	95.57	95.37
	PubFig	99.99	99.27	99.63	99.63
PubFig	MEDS	99.86	99.86	99.86	99.86
	Multi-PIE	100.00	100.00	100.00	100.00

TABLE 2

Recall, Precision, F1, and Accuracy Scores (%) of Crossing Model Experiments.

Training	Testing	Dataset	Recall	Precision	F1	Accuracy
VGG-16	GoogleNet	MEDS	100.00	97.00	98.48	98.46
		Multi-PIE	100.00	99.74	99.87	99.87
		PubFig	99.47	99.83	99.65	99.65
VGG-16	CaffeNet	MEDS	90.45	96.99	93.61	93.82
		Multi-PIE	100.00	99.74	99.87	99.87
		PubFig	98.78	99.83	99.30	99.30

between TDSC'20 and other competing methods becomes smaller. This implies that the simple decision-level fusion of global and local orthogonal transforms in TDSC'20 cannot handle more complex detection tasks well. It should be considered as an inflexible remedy for the contradiction of spatial and frequency discriminability. In general, our method still achieves $\sim 5\%$ gain w.r.t. TDSC'20 and $\sim 10\%$ gain w.r.t. other competing methods.

The above consistent performance gains in Figs. 5 \sim 9 validate the advanced nature of the proposed detector, revealing the potential of our spatial-frequency discriminative decomposition in perturbation detection tasks.

6.3 Crossing Experiments

Through above benchmark experiments, we have positioned our detector w.r.t. some state-of-the-art detectors. Such extensive results indicate a consistent performance advantage of the proposed method under the typical experiment protocol. In this part, we will further analyze whether the above performance advantage arises from a certain overfitting. More specifically, we will test a trained detector by crossing to other similar experiment protocols, thereby quantifying its transferability to reasonable changes.

6.3.1 Crossing Dataset

Table 1 lists the various performance scores of the proposed detector on crossing dataset protocol with universal perturbation. Here, the protocol involves three face datasets: MEDS, Multi-PIE, and PubFig. In general, a promising detector is expected to be generalizable to such natural differences of the training and testing phases. As can be observed here, our detector exhibits consistent recall, precision, F1, and accuracy scores for all crossing dataset scenarios, where most cases (except for Multi-PIE to MEDS) the

TABLE 3

Recall, Precision, F1, and Accuracy Scores (%) of Crossing Attack Experiments.

Training	Testing	Recall	Precision	F1	Accuracy
BIM	FGSM	100.00	100.00	100.00	100.00
	PGD	100.00	99.98	99.99	99.99
	FAB	84.82	99.53	91.59	92.21
	Square	78.82	99.50	87.96	89.21
FGSM	BIM	99.98	99.86	99.92	99.92
	PGD	100.00	99.86	99.93	99.93
	FAB	76.90	99.82	86.87	88.38
	Square	77.48	99.82	87.24	88.67
PGD	BIM	100.00	99.86	99.93	99.93
	FGSM	100.00	99.86	99.93	99.93
	FAB	80.28	99.83	88.99	90.07
	Square	78.70	99.82	88.01	89.28
FAB	BIM	100.00	99.11	99.55	99.55
	FGSM	100.00	99.11	99.55	99.55
	PGD	100.00	99.11	99.55	99.55
	Square	79.06	98.87	87.86	89.08
Square	BIM	100.00	98.68	99.33	99.33
	FGSM	100.00	98.78	99.38	99.38
	PGD	100.00	98.48	99.24	99.23
	FAB	89.14	98.52	93.60	93.90

scores are even $\sim 100\%$. The worst case is mainly due to the fact that Multi-PIE has less data diversity than MEDS, leading to insufficient learning; the reverse of the two datasets significantly improves the scores. This numerical evidence suggests that our spatial-frequency discriminative decomposition provides complete and intrinsic features of adversarial perturbations, and therefore generalizes well to unseen-but-similar datasets.

Remark. In addition, we would like to provide some supplementary information as comparison baselines. Based on scores reported in the literature, competing algorithms arXiv'17 and TDSC'18 achieve $\sim 80\%$ accuracy scores on the crossing dataset protocol from MEDS to Multi-PIE, and $\sim 70\%$ accuracy scores for the reverse protocol. Thus they exhibit a $> 20\%$ performance gap w.r.t. the proposed detector. It is further verified that the proposed decomposition serves as a more generic representation than such simple filters.

6.3.2 Crossing Model

In Table 2, we provide the various performance scores of the proposed detector on crossing model protocol with universal perturbation. Here, our detector is trained on VGG-16 and tested on GoogleNet or CaffeNet, where the training and testing are also considered on three face datasets. Note that although the adversarial perturbations on different models differ significantly at the numerical level, they still exhibit specific statistical consistency; the mining of this consistency largely reflects the generalizability of the detector. Obviously, the proposed detector remains stable, regardless of the different datasets and the different performance metrics. For most cases, our detector exhibits $\sim 100\%$ scores, and even the worst case (VGG-16 to CaffeNet on MEDS) is

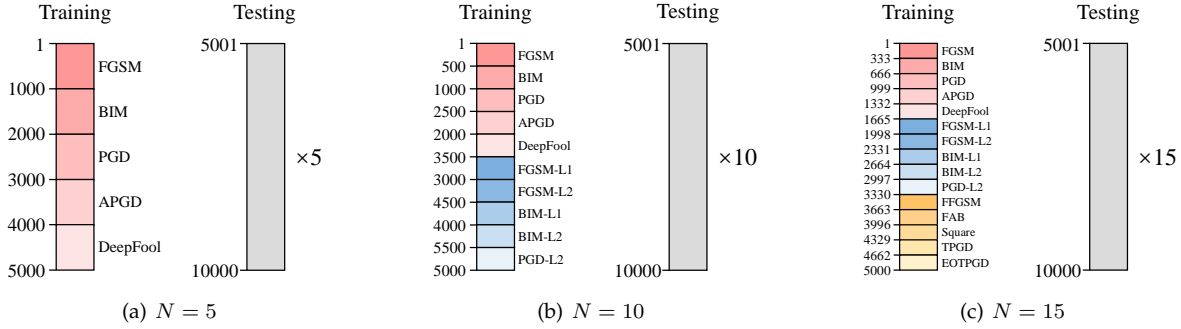


Fig. 10. Illustration for the adversarial image division in challenging experiments. Note that the more attacks involved, the fewer training examples for each attack, and therefore this protocol is a comprehensive challenge for the discriminability, generalization, completeness, and efficiency of the detector.

still 93.82%. These consistent phenomena suggest that the proposed detector and its foundational decomposition have well generalizability to unseen-but-similar models.

Remark. In addition, we would like to provide some supplementary information as comparison baselines. Based on scores reported in the literature, competing algorithm TDSC’20 achieves $\sim 93\%$ accuracy score on the crossing model protocol from VGG-16 to GoogleNet on MEDS, and $\sim 96\%$ accuracy score for the similar protocol on Multi-PIE. Therefore, our detector still exhibits gains w.r.t. this orthogonal transform based detector.

6.3.3 Crossing Attack

As for Table 3, we list the various performance scores of the proposed detector on crossing attack protocol on MNIST dataset. Here, the protocol involves five attacks, i.e., BIM, FGSM, PGD, FAB, and Square, with quite significant differences in their designs. The experiment will consider any crossing pair of these five attacks in training and testing, for a total of 20 pairs. As can be expected, the adversarial perturbations derived from these attacks are different numerically, but meanwhile have similar statistical properties. In the table, the extensive performance scores indicate that the proposed detector is capable of representing the statistical consistency over such attacks. For 12 crossing pairs, our detector exhibits $\sim 100\%$ scores of F1 and accuracy. For the worst case, the F1 and accuracy scores of our detector are still $\sim 87\%$. In general, the performance of the proposed detector is quite promising, even w.r.t. the generalizability of the unseen and somewhat different adversarial perturbations.

Remark. In addition, we would like to provide some supplementary information as comparison baselines. Based on scores reported in the literature, competing algorithms arXiv’17, ICLR’18, TDSC’18, CVPR’19, and TDSC’20 achieve $\sim 64\%$, $\sim 76\%$, $\sim 65\%$, $\sim 68\%$, and $\sim 95\%$ average accuracy scores over FGSM-like crossing pairs, respectively. In Table 3, our algorithm exhibits an average accuracy score of $\sim 96\%$. Note that even though our protocol involves more diverse attacks, the proposed detector still provides better scores than above competing methods.

The above consistent performance gains in Tables 1 \sim 3 validate the advanced nature of the proposed detector, revealing the generalizability of our spatial-frequency discriminative decomposition for unseen-but-similar scenarios.

6.4 Challenging Experiments

The above benchmarking and crossing experiments have extensively demonstrated the advantages of the proposed detector over state-of-the-art detectors under ideal protocols. In this part, we turn to more challenging protocols. Such protocols can verify the discriminability, generalization, completeness, and efficiency of the proposed detectors in a comprehensive and realistic manner.

6.4.1 From Ideal to Practice

We begin with a discussion on the practical deployment of the adversarial perturbation detector and the corresponding training strategy. In real-world scenarios, it is expected that the detector enables an accurate and generic defense for the widest possible range of adversarial attacks. In general, two training and deployment approaches exist to achieve this goal:

- *Integration during inference.* Multiple detectors are involved here, each of which is trained on adversarial examples from only one attack. When deployed, the example under analysis is filled into these detectors separately, and the corresponding results are then integrated as the final prediction. Therefore, this approach can be construed as a late integration strategy.
- *Integration during training.* Only one detector is involved here, which is trained directly on adversarial examples from the widest possible range of attacks. After training, the detector is deployed directly to predict arbitrary examples. Therefore, this approach can be construed as an early fusion strategy.

It is clear that the integration during training is more compact. Compared to the integration during inference, it will consume significantly fewer computational resources in deployment, while not involving tricky integration policy design for the results from multiple detectors. However, most of the benchmarking and crossing experiments in the literature are trained only with single kind of attack, and thus only verifying the effectiveness for the integration during inference. Therefore, we not only consider benchmarking and crossing experiments for the integration during inference (Sections 6.2 and 6.3), but will also focus on more challenging experiments for the integration during training (Section 6.4).

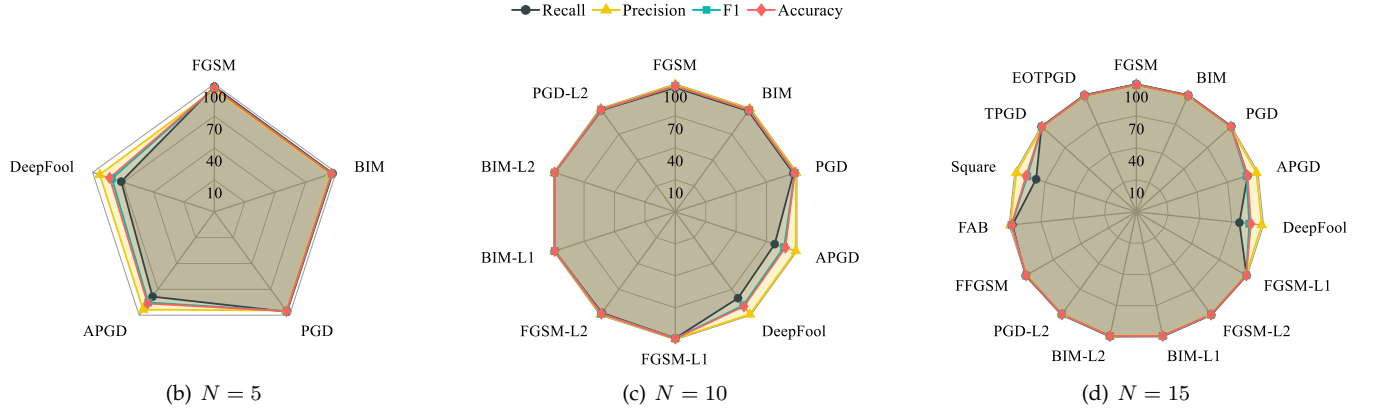


Fig. 11. Recall, precision, F1, and accuracy scores (%) of challenging experiments. Note that the proposed detector performs consistently even with more attacks and fewer training examples, verifying its discriminability, generalization, completeness, and efficiency.

6.4.2 A Comprehensive and Realistic Protocol

For a comprehensive investigation of the proposed detector in the scenario of integration during training, we design the following experimental protocol. We selected 10000 original images in MNIST for generating the experimental images, in which the first/latter 5000 images are used to derive the training/testing examples respectively. Assuming that N attacks are considered, where $N = 5, 10, 15$ in our experiments. For the training, the first 5000 images are equally divided into N parts for generating the adversarial images corresponding to per attack, and then they are used as training examples together with the first 5000 original images. Our detector will be trained directly on such 10000 images. For the testing, the examples under each attack will consist of the latter 5000 original images and 5000 corresponding adversarial images, resulting in a total of $N \times 10000$ testing examples.

In Fig. 10, we present an illustration for the above adversarial image division w.r.t. $N = 5, 10, 15$. Note that when N increases, the number of adversarial images from each attack in the training set, i.e., $5000/N$, will decrease, while the counterpart in the testing set remains 5000. Obviously, this protocol is a comprehensive challenge for the discriminability, generalization, completeness, and efficiency of the detector.

In Fig. 11, we show the various performance scores of the proposed detector on challenging experiment protocol. Here, corresponding to Fig. 10, the protocol involves increasing number of attacks and decreasing number of training examples from (a) to (c). In general, a promising detector is expected to be stable to realistic variations in the problem complexity or the training scale. As can be observed here, our detector exhibits consistent recall, precision, F1, and accuracy scores on all three scenarios (a) \sim (c). For the most challenging scenario (c), where number of attacks is 15 and number of training adversarial images per attack is only 333, the scores w.r.t. most attacks (except for APGD, DeepFool, and Square) are even $\sim 100\%$. The worst case is DeepFool with $\sim 87\%$ scores of F1 and accuracy. Such scores are still generally satisfactory, considering the training/testing adversarial images ratio is 300/5000. The above phenomenon suggests that our detector and its foundational decomposition have:

- Discriminability for a wide range of attacks;
- Generalization for unseen-but-similar examples;
- Completeness for potential perturbation patterns;
- Efficiency on training scale.

Starting from such properties, the proposed detector can be regarded as a more comprehensive and effective defense for the realistic scenarios with integration during training.

7 CONCLUSION

In general, our main goal is to provide a more comprehensive design of adversarial perturbation detector. As a technical foundation of the detector, we have proposed the spatial-frequency discriminative decomposition with secret keys, motivated by the accuracy and security issues of existing detectors. Here, the accuracy and security ingredients in this paper can be summarized as follows.

- Regarding the *accuracy*, we attribute the accuracy bottleneck of existing detectors to the fundamental contradiction of spatial and frequency discriminability in the decomposition. Specifically, the non-orthogonal decomposition (e.g., SRM) is not sufficient to completely represent a wide range of potential perturbations. The global (e.g., DST) or local (e.g., DWT) orthogonal decomposition cannot mine both frequency and spatial priors (Propositions 3 and 4), thereby failing to fully reveal the statistical regularity (Proposition 2). In this paper, we have introduced the Krawtchouk basis (Definition 2) for more discriminative decomposition, providing a mid-scale representation with rich spatial-frequency information (Property 1). The resulting detector is therefore claimed to have better discriminability in the decomposition of natural images and adversarial perturbations (Main Result 1).
- Regarding the *security*, we attribute the successful defense-aware (secondary) attack to the transparency of detector-interested features for the attacker. With such knowledge, the attacker can regenerate adversarial perturbations without exhibiting obvious artifacts on these features (Propositions 5 and 6). In this paper, we have proposed the random feature

selection for de-transparency, where a key controlled pseudorandom number generator determines the spatial and frequency parameters of the decomposition. The resulting detector is therefore claimed to be secure against the defense-aware attack: it is difficult (or impossible) to divide between to-be-attacked and to-be-evaded features even with the knowledge of the detector other than the keys (Main Result 2).

We have provided statistical comparisons with state-of-the-art detectors, by the benchmarking (Section 6.2), crossing (Section 6.3), and challenging (Section 6.4) experiments for both ideal and realistic scenarios (w.r.t. integration during inference and training). In general, such extensive experimental results confirm the effectiveness of our detector, exhibiting quite satisfactory discriminability, generalization, completeness, and efficiency w.r.t. existing works.

Our future work will focus on more formal statistical analysis for the decomposition of natural images and adversarial perturbations, potentially involving coefficient statistical modeling and hypothesis testing.

REFERENCES

- [1] Y. Bengio, A. Courville, and P. Vincent, "Representation learning: A review and new perspectives," *IEEE Trans. Pattern Anal. Mach. Intell.*, vol. 35, no. 8, pp. 1798–1828, 2013.
- [2] L. Zhao, Q. Wang, C. Wang, Q. Li, C. Shen, and B. Feng, "Veriml: Enabling integrity assurances and fair payments for machine learning as a service," *IEEE Trans. Parallel Distrib. Syst.*, vol. 32, no. 10, pp. 2524–2540, 2021.
- [3] J. M. Wing, "Trustworthy AI," *Commun. ACM*, vol. 64, no. 10, pp. 64–71, 2021.
- [4] A. Fawzi, S.-M. Moosavi-Dezfooli, and P. Frossard, "The robustness of deep networks: A geometrical perspective," *IEEE Signal Process Mag.*, vol. 34, no. 6, pp. 50–62, 2017.
- [5] I. Goodfellow, P. McDaniel, and N. Papernot, "Making machine learning robust against adversarial inputs," *Commun. ACM*, vol. 61, no. 7, pp. 56–66, 2018.
- [6] C. Szegedy, W. Zaremba, I. Sutskever, J. Bruna, D. Erhan, I. Goodfellow, and R. Fergus, "Intriguing properties of neural networks," in *Proc. Int. Conf. Learn. Represent.*, 2014.
- [7] A. Kurakin, I. Goodfellow, and S. Bengio, "Adversarial examples in the physical world," in *Artificial intelligence safety and security*. Chapman and Hall/CRC, 2018, pp. 99–112.
- [8] J. Su, D. V. Vargas, and K. Sakurai, "One pixel attack for fooling deep neural networks," *IEEE Trans. Evol. Comput.*, vol. 23, no. 5, pp. 828–841, 2019.
- [9] I. Goodfellow, J. Shlens, and C. Szegedy, "Explaining and harnessing adversarial examples," in *Proc. Int. Conf. Learn. Represent.*, 2015.
- [10] N. Carlini and D. Wagner, "Towards evaluating the robustness of neural networks," in *Proc. IEEE Symp. Secur. Priv.*, 2017, pp. 39–57.
- [11] S.-M. Moosavi-Dezfooli, A. Fawzi, O. Fawzi, and P. Frossard, "Universal adversarial perturbations," in *Proc. IEEE Conf. Comput. Vis. Pattern Recognit.*, 2017, pp. 1765–1773.
- [12] P.-Y. Chen, H. Zhang, Y. Sharma, J. Yi, and C.-J. Hsieh, "Zoo: Zeroth order optimization based black-box attacks to deep neural networks without training substitute models," in *Proc. ACM Workshop Artif. Intell. Secur.*, 2017, pp. 15–26.
- [13] K. Eykholt, I. Evtimov, E. Fernandes, B. Li, A. Rahmati, C. Xiao, A. Prakash, T. Kohno, and D. Song, "Robust physical-world attacks on deep learning visual classification," in *Proc. IEEE Conf. Comput. Vis. Pattern Recognit.*, 2018, pp. 1625–1634.
- [14] M. Andriushchenko and N. Flammarion, "Understanding and improving fast adversarial training," *Proc. Conf. Neural Inf. Proces. Syst.*, vol. 33, pp. 16 048–16 059, 2020.
- [15] H. Liu, Y. Wang, W. Fan, X. Liu, Y. Li, S. Jain, Y. Liu, A. Jain, and J. Tang, "Trustworthy AI: A computational perspective," *ACM Trans. Intell. Syst. Technol.*, vol. 14, no. 1, pp. 1–59, 2022.
- [16] C. Xiang, A. N. Bhagoji, V. Sehwag, and P. Mittal, "PatchGuard: A provably robust defense against adversarial patches via small receptive fields and masking," in *Proc. USENIX Secur. Symp.*, 2021, pp. 2237–2254.
- [17] A. Nayebi and S. Ganguli, "Biologically inspired protection of deep networks from adversarial attacks," *arXiv preprint arXiv:1703.09202*, 2017.
- [18] A. Ross and F. Doshi-Velez, "Improving the adversarial robustness and interpretability of deep neural networks by regularizing their input gradients," in *Proc. AAAI Conf. Artif. Intell.*, vol. 32, no. 1, 2018.
- [19] H. Zhang, Y. Yu, J. Jiao, E. Xing, L. El Ghaoui, and M. Jordan, "Theoretically principled trade-off between robustness and accuracy," in *Proc. Int. Conf. Mach. Learn.*, 2019, pp. 7472–7482.
- [20] X. Zhang, X. Zheng, and W. Mao, "Adversarial perturbation defense on deep neural networks," *ACM Comput. Surv.*, vol. 54, no. 8, pp. 1–36, 2021.
- [21] S. Qi, Y. Zhang, C. Wang, J. Zhou, and X. Cao, "A principled design of image representation: Towards forensic tasks," *IEEE Trans. Pattern Anal. Mach. Intell.*, 2022.
- [22] G.-L. Chen and C.-C. Hsu, "Jointly defending DeepFake manipulation and adversarial attack using decoy mechanism," *IEEE Trans. Pattern Anal. Mach. Intell.*, 2023.
- [23] B. Liang, H. Li, M. Su, X. Li, W. Shi, and X. Wang, "Detecting adversarial image examples in deep neural networks with adaptive noise reduction," *IEEE Trans. Dependable Secure Comput.*, vol. 18, no. 1, pp. 72–85, 2018.
- [24] J. Liu, W. Zhang, Y. Zhang, D. Hou, Y. Liu, H. Zha, and N. Yu, "Detection based defense against adversarial examples from the steganalysis point of view," in *Proc. IEEE Conf. Comput. Vis. Pattern Recognit.*, 2019, pp. 4825–4834.
- [25] A. N. Bhagoji, D. Cullina, C. Sitawarin, and P. Mittal, "Enhancing robustness of machine learning systems via data transformations," in *Proc. Annu. Conf. Inf. Sci. Syst.*, 2018, pp. 1–5.
- [26] N. Akhtar, J. Liu, and A. Mian, "Defense against universal adversarial perturbations," in *Proc. IEEE Conf. Comput. Vis. Pattern Recognit.*, 2018, pp. 3389–3398.
- [27] A. Agarwal, R. Singh, M. Vatsa, and N. Ratha, "Image transformation-based defense against adversarial perturbation on deep learning models," *IEEE Trans. Dependable Secure Comput.*, vol. 18, no. 5, pp. 2106–2121, 2020.
- [28] A. Agarwal, G. Goswami, M. Vatsa, R. Singh, and N. K. Ratha, "Damad: Database, attack, and model agnostic adversarial perturbation detector," *IEEE Trans. Neural Networks Learn. Syst.*, vol. 33, no. 8, pp. 3277–3289, 2021.
- [29] J.-H. Hoepman and B. Jacobs, "Increased security through open source," *Commun. ACM*, vol. 50, no. 1, pp. 79–83, 2007.
- [30] S. G. Mallat, "A theory for multiresolution signal decomposition: the wavelet representation," *IEEE Trans. Pattern Anal. Mach. Intell.*, vol. 11, no. 7, pp. 674–693, 1989.
- [31] Z. Chen, B. Tondi, X. Li, R. Ni, Y. Zhao, and M. Barni, "Secure detection of image manipulation by means of random feature selection," *IEEE Trans. Inf. Forensics Secur.*, vol. 14, no. 9, pp. 2454–2469, 2019.
- [32] T. Miyato, S.-i. Maeda, M. Koyama, and S. Ishii, "Virtual adversarial training: a regularization method for supervised and semi-supervised learning," *IEEE Trans. Pattern Anal. Mach. Intell.*, vol. 41, no. 8, pp. 1979–1993, 2018.
- [33] X. Jia, X. Wei, X. Cao, and X. Han, "Adv-watermark: A novel watermark perturbation for adversarial examples," in *Proc. ACM Int. Conf. Multimed.*, 2020, pp. 1579–1587.
- [34] L. Zhai, F. Juefei-Xu, Q. Guo, X. Xie, L. Ma, W. Feng, S. Qin, and Y. Liu, "It's raining cats or dogs? adversarial rain attack on DNN perception," *arXiv preprint arXiv:2009.09205*, vol. 2, 2020.
- [35] Q. Guo, Z. Cheng, F. Juefei-Xu, L. Ma, X. Xie, Y. Liu, and J. Zhao, "Learning to adversarially blur visual object tracking," in *Proc. IEEE Int. Conf. Comput. Vis.*, 2021, pp. 10 839–10 848.
- [36] S. Zhang, H. Gao, and Q. Rao, "Defense against adversarial attacks by reconstructing images," *IEEE Trans. Image Process.*, vol. 30, pp. 6117–6129, 2021.
- [37] N. Das, M. Shanbhogue, S.-T. Chen, F. Hohman, S. Li, L. Chen, M. E. Kounavis, and D. H. Chau, "Shield: Fast, practical defense and vaccination for deep learning using JPEG compression," in *Proc. ACM SIGKDD Int. Conf. Knowl. Discov. Data Min.*, 2018, pp. 196–204.
- [38] Y. Zhang and P. Liang, "Defending against whitebox adversarial attacks via randomized discretization," in *Proc. Int. Conf. Artif. Intell. Stat.*, 2019, pp. 684–693.
- [39] S. Rifai, P. Vincent, X. Muller, X. Glorot, and Y. Bengio, "Contractive auto-encoders: Explicit invariance during feature extraction," in *Proc. Int. Conf. Mach. Learn.*, 2011, pp. 833–840.

[40] X.-H. Li, C. C. Cao, Y. Shi, W. Bai, H. Gao, L. Qiu, C. Wang, Y. Gao, S. Zhang, X. Xue *et al.*, "A survey of data-driven and knowledge-aware eXplainable AI," *IEEE Trans. Knowl. Data Eng.*, vol. 34, no. 1, pp. 29–49, 2020.

[41] S. Han, C. Lin, C. Shen, Q. Wang, and X. Guan, "Interpreting adversarial examples in deep learning: A review," *ACM Comput. Surv.*, 2023.

[42] T. Tanay and L. Griffin, "A boundary tilting perspective on the phenomenon of adversarial examples," *arXiv preprint arXiv:1608.07690*, 2016.

[43] D. Yin, R. Gontijo Lopes, J. Shlens, E. D. Cubuk, and J. Gilmer, "A Fourier perspective on model robustness in computer vision," *Proc. Adv. neural inf. proces. syst.*, vol. 32, 2019.

[44] A. Ilyas, S. Santurkar, D. Tsipras, L. Engstrom, B. Tran, and A. Madry, "Adversarial examples are not bugs, they are features," *Proc. Adv. neural inf. proces. syst.*, vol. 32, 2019.

[45] Z. Zha, X. Yuan, J. Zhou, C. Zhu, and B. Wen, "Image restoration via simultaneous nonlocal self-similarity priors," *IEEE Trans. Image Process.*, vol. 29, pp. 8561–8576, 2020.

[46] S. Qi, Y. Zhang, C. Wang, J. Zhou, and X. Cao, "A survey of orthogonal moments for image representation: theory, implementation, and evaluation," *ACM Comput. Surv.*, vol. 55, no. 1, pp. 1–35, 2021.

[47] P.-T. Yap, R. Paramesran, and S.-H. Ong, "Image analysis by Krawtchouk moments," *IEEE Trans. Image Process.*, vol. 12, no. 11, pp. 1367–1377, 2003.

[48] H. Yang, S. Qi, J. Tian, P. Niu, and X. Wang, "Robust and discriminative image representation: Fractional-order Jacobi-Fourier moments," *Pattern Recognit.*, vol. 115, p. 107898, 2021.

[49] Y. LeCun, L. Bottou, Y. Bengio, and P. Haffner, "Gradient-based learning applied to document recognition," *Proc. IEEE*, vol. 86, no. 11, pp. 2278–2324, 1998.

[50] K. Simonyan and A. Zisserman, "Very deep convolutional networks for large-scale image recognition," in *Proc. Int. Conf. Learn. Represent.*, 2015.

[51] C. Szegedy, W. Liu, Y. Jia, P. Sermanet, S. Reed, D. Anguelov, D. Erhan, V. Vanhoucke, and A. Rabinovich, "Going deeper with convolutions," in *Proc. IEEE Conf. Comput. Vis. Pattern Recognit.*, 2015, pp. 1–9.

[52] Y. Jia, E. Shelhamer, J. Donahue, S. Karayev, J. Long, R. Girshick, S. Guadarrama, and T. Darrell, "Caffe: Convolutional architecture for fast feature embedding," in *Proc. ACM Int. Conf. Multimed.*, 2014, pp. 675–678.

[53] Y. LeCun, C. Corinna, and J. B. Christopher, "MNIST," <http://yann.lecun.com/exdb/mnist/>.

[54] A. Krizhevsky, V. Nair, and G. Hinton, "CIFAR-10," <https://www.cs.toronto.edu/~kriz/cifar.html>.

[55] A. Founds, N. Orlans, G. Whiddon, and C. Watson, "MEDS," <https://www.nist.gov/itl/iad/image-group/special-database-32-multiple-encounter-dataset-meds>.

[56] R. Gross, I. Matthews, J. Cohn, T. Kanade, and S. Baker, "Multi-PIE," <https://www.cs.cmu.edu/afs/cs/project/PIE/MultiPie/Multi-Pie/Home.html>.

[57] N. Kumar, A. C. Berg, P. N. Belhumeur, and S. K. Nayar, "PubFig," <https://www.cs.columbia.edu/CAVE/databases/pubfig/>.

[58] J. Deng, W. Dong, R. Socher, L.-J. Li, K. Li, and L. Fei-Fei, "ImageNet," <https://www.image-net.org/index.php>.

[59] A. Madry, A. Makelov, L. Schmidt, D. Tsipras, and A. Vladu, "Towards deep learning models resistant to adversarial attacks," in *Proc. Int. Conf. Learn. Represent.*, 2018.

[60] F. Croce and M. Hein, "Reliable evaluation of adversarial robustness with an ensemble of diverse parameter-free attacks," in *Proc. Int. Conf. Mach. Learn.*, 2020, pp. 2206–2216.

[61] S.-M. Moosavi-Dezfooli, A. Fawzi, and P. Frossard, "Deepfool: a simple and accurate method to fool deep neural networks," in *Proc. IEEE Conf. Comput. Vis. Pattern Recognit.*, 2016, pp. 2574–2582.

[62] E. Wong, L. Rice, and J. Z. Kolter, "Fast is better than free: Revisiting adversarial training," in *Proc. Int. Conf. Learn. Represent.*, 2020.

[63] F. Croce and M. Hein, "Minimally distorted adversarial examples with a fast adaptive boundary attack," in *Proc. Int. Conf. Mach. Learn.*, 2020, pp. 2196–2205.

[64] M. Andriushchenko, F. Croce, N. Flammarion, and M. Hein, "Square attack: a query-efficient black-box adversarial attack via random search," in *Proc. Eur. Conf. Comput. Vis.*, 2020, pp. 484–501.

[65] H. Zhang, Y. Yu, J. Jiao, E. Xing, L. El Ghaoui, and M. Jordan, "Theoretically principled trade-off between robustness and accuracy," in *Proc. Int. Conf. Mach. Learn.*, 2019, pp. 7472–7482.

[66] R. S. Zimmermann, "Comment on 'Adv-BNN: Improved adversarial defense through robust Bayesian Neural Network,'" *arXiv preprint arXiv:1907.00895*, 2019.

[67] K. R. Mopuri, U. Garg, and R. V. Babu, "Fast Feature Fool: A data independent approach to universal adversarial perturbations," in *Proc. Br. Mach. Vis. Conf.*, 2017.

[68] R. Feinman, R. R. Curtin, S. Shintre, and A. B. Gardner, "Detecting adversarial samples from artifacts," *arXiv preprint arXiv:1703.00410*, 2017.

[69] S. Liang, Y. Li, and R. Srikant, "Principled detection of out-of-distribution examples in neural networks," in *Proc. Int. Conf. Learn. Represent.*, 2018.

[70] G. Goswami, A. Agarwal, N. Ratha, R. Singh, and M. Vatsa, "Detecting and mitigating adversarial perturbations for robust face recognition," *Int. J. Comput. Vision*, vol. 127, pp. 719–742, 2019.

[71] S. Ma, Y. Liu, G. Tao, W.-C. Lee, and X. Zhang, "Nic: Detecting adversarial samples with neural network invariant checking," in *Proc. Net. Distribut. Sys. Secur. Symp.*, 2019.



Chao Wang received the B.S. and M.S. degrees from Liaoning Normal University, Dalian, China, in 2017 and 2020, respectively. She is currently pursuing the Ph.D. degree in computer science at Nanjing University of Aeronautics and Astronautics, Nanjing, China.

She has authored or coauthored academic papers in top-tier venues including *IEEE Transactions on Information Forensics and Security* and *IEEE Transactions on Pattern Analysis and Machine Intelligence*. Her research interests include trustworthy artificial intelligence, adversarial learning, and media forensics.



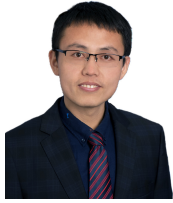
Shuren Qi received the B.A. and M.E. degrees from Liaoning Normal University, Dalian, China, in 2017 and 2020, respectively. He is currently pursuing the Ph.D. degree in computer science with Nanjing University of Aeronautics and Astronautics, Nanjing, China.

He has authored or coauthored academic papers in top-tier venues including *ACM Computing Surveys* and *IEEE Transactions on Pattern Analysis and Machine Intelligence*. His research interests include invariant feature extraction and visual signal representation with applications in robust pattern recognition and media forensics/security.



Zhiqiu Huang received the Ph.D. degree in computer science from Nanjing University of Aeronautics and Astronautics, Nanjing, China, in 1999.

He is a professor with the College of Computer Science and Technology, Nanjing University of Aeronautics and Astronautics, China. He has authored or coauthored more than 80 journal and conference papers. His research interests include software engineering, formal methods, and knowledge engineering.



Yushu Zhang (Senior Member, IEEE) received the Ph.D. degree in computer science from Chongqing University, Chongqing, China, in 2014.

He held various research positions with the City University of Hong Kong, Southwest University, University of Macau, and Deakin University. He is a Professor with the College of Computer Science and Technology, Nanjing University of Aeronautics and Astronautics, Nanjing, China. His research interests include multimedia processing and security, artificial intelligence, and blockchain.

Dr. Zhang is an Associate Editor of *Signal Processing and Information Sciences*.



Xiaochun Cao (Senior Member, IEEE) received the B.E. and M.E. degrees in computer science from Beihang University, Beijing, China, in 1999 and 2002, respectively, and the Ph.D. degree in computer science from the University of Central Florida, Orlando, FL, USA, in 2006.

After graduation, he spent about three years at ObjectVideo Inc., as a Research Scientist. From 2008 to 2012, he was a Professor at Tianjin University, Tianjin, China. Before joining Sun Yat-sen University, Shenzhen, China, he was a

Professor at the Institute of Information Engineering, Chinese Academy of Sciences, Beijing, China. He is a Professor and the Dean with the School of Cyber Science and Technology, Shenzhen Campus of Sun Yat-sen University. He has authored or coauthored more than 200 journal and conference papers.

Dr. Cao's dissertation was nominated for the University Level Outstanding Dissertation Award. He was a recipient of the Piero Zamparoni Best Student Paper Award at the *International Conference on Pattern Recognition*, in 2004 and 2010. He was on the Editorial Boards of *IEEE Transactions on Circuits and Systems for Video Technology* and *IEEE Transactions on Multimedia*. He is on the Editorial Boards of *IEEE Transactions on Pattern Analysis and Machine Intelligence* and *IEEE Transactions on Image Processing*.